

Coupling of tsunami generation and propagation codes

Philip Watts¹, Stephan T. Grilli², and Fumihiko Imamura³

¹*Applied Fluids Engineering, Inc., Long Beach, California, U.S.A.*

²*Department of Ocean Engineering, University of Rhode Island, Narragansett, Rhode Island, U.S.A.*

³*Disaster Control Research Center, Tohoku University, Aoba, Sendai, Japan*

Abstract. Tsunami generation by underwater landslides has been simulated with a variety of numerical models. We propose a benchmark case that enables validation of tsunami generation models. We compare experimental benchmark results with results from a boundary element method tsunami generation code. Our simulation approximates an underwater slide as a solid body. In order to justify this approximation, we show that center of mass motion governs tsunami generation. We also show that deformation is of secondary consideration for tsunamis generated by underwater slides. Given the computational cost of complete fluid dynamic simulations, a method is sought to combine the tsunami generation code with a tsunami propagation code. We develop a coupled model that employs an irrotational, inviscid boundary element code in the near-field and the depth-averaged nonlinear wave propagation code in the far-field. A case study of the 1998 Papua New Guinea tsunami demonstrates the effectiveness of the coupled model approach.

1. Introduction

Landslide tsunamis are receiving significantly more attention following surveys and analyses demonstrating that the surprisingly large local tsunami that struck Papua New Guinea (PNG) in 1998 was generated by an underwater slump (Kawata *et al.*, 1999; Tappin *et al.*, 1999, 2001; Synolakis *et al.*, 2001). In response to these and other studies, recent work by marine geologists now considers the tsunamigenic potential of landslide scars (Goldfinger *et al.*, 2000; Driscoll *et al.*, 2000). Despite these advances in the observational science, there are few validations of the numerical models currently in use (Watts *et al.*, 2000; Grilli and Watts, 2001). Consequently, the ability of scientists to simulate landslide tsunamis remains in doubt.

Researchers have tackled landslide tsunami generation with a wide variety of numerical methods incorporating many different assumptions. Iwasaki (1987, 1997) and Verriere and Lenoir (1992) utilized linear potential theory to simulate wave generation by moving the domain boundary. Depth-averaged shallow water wave equations were simulated by Fine *et al.* (1998), Harbitz (1992), Imamura and Gica (1996), Imamura and Imteaz (1995), and Jiang and LeBlond (1992, 1993, 1994) in combination with disparate landslide models. Fully nonlinear fluid dynamic field equations were solved

¹Applied Fluids Engineering, Inc., 5710 East 7th Street, PMB #237, Long Beach, CA 90803, U.S.A. (phil.watts@appliedfluids.com)

²Sheets Building, Department of Ocean Engineering, Narragansett Bay Campus, University of Rhode Island, Narragansett, RI 02882, U.S.A. (grilli@oce.uri.edu)

³Disaster Control Research Center, School of Engineering, Tohoku University, Aoba 06, Sendai, 980-8579, Japan (imamura@tsunami2.civil.tohoku.ac.jp)

by Assier Rzadkiewicz *et al.* (1997), Grilli and Watts (1999), and Heinrich (1992) in concert with assorted landslide models. For the most part, scientists have studied vastly different landslide geometries, motions, and constitutive behaviors. There is currently no consensus on the ability of these different models to reproduce landslide tsunamis.

Watts *et al.* (2000, 2001) appear to be the only researchers to compare tsunami generation for both different center of mass motions and different rates of deformation. They show that center of mass motion is the most important determinant of tsunami features. They also attempt to discern the effect of depth-averaged wave equations on tsunami generation. They conclude that depth averaging may diminish tsunami amplitude by restricting fluid flow to uniform horizontal motions. We will revisit these results here for the sake of completeness. We endeavor to address three questions in this paper. With such a wide variety of models available, can any single model be used reliably for both landslide tsunami generation and propagation? If not, what are the most important tsunami generation features to simulate? Last of all, how should tsunami generation and propagation codes be coupled?

2. Tsunami Sources

Coseismic displacement and mass failure constitute the two most common forms of tsunami generation. Coseismic displacement, or vertical seafloor deformation, occurs during most earthquakes and often generates tsunamis with longer wavelengths, longer periods, and a larger source area than those generated by mass failures (Hammack, 1973; Watts, 1998, 2000). Hence, coseismic displacement readily produces transoceanic tsunamis, whereas mass failures produce tsunamis that decay rapidly away from the axis of failure (Plafker *et al.*, 1969; Iwasaki, 1997). Coseismic displacement generates tsunami amplitudes that correlate with earthquake magnitude (Hammack, 1973; Geist, 1998); submarine mass failures produce tsunamis with amplitudes limited only by the vertical extent of center of mass motion (Murty, 1979; Watts, 1998). Both mass failure center of mass motion and tsunami generation can surpass those of coseismic displacement by orders of magnitude, posing a greater threat to coastal communities than previously recognized.

Submarine mass failure or underwater landslide are broad terms encompassing reef failure, rock slides, noncohesive slides, cohesive slumps, and other related events. There is a spectrum of mass failure materials that each possess distinct modes of failure and subsequent behaviors (Prior and Coleman, 1979; Edgers and Karlsrud, 1982; Hampton *et al.*, 1996). Any submerged geological structure can be expected to undergo some degree of submarine mass failure due to strong ground motion from a nearby earthquake (Tappin *et al.*, 1999, 2001). As such, all forms of submarine mass failure can be present at the same time. Despite the ubiquity of mass failure, most events are not tsunamigenic on account of their small size or deep submergence. Here, the focus will be on two idealized forms of mass movement: noncohesive slides and cohesive slumps (Watts and Borrero, this volume).

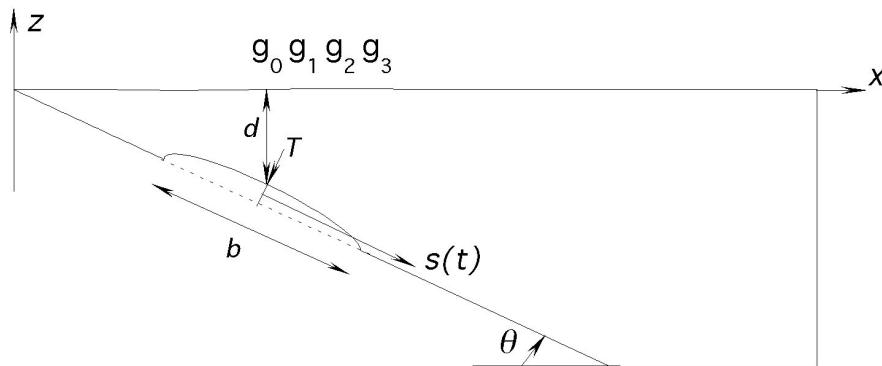


Figure 1: Schematic diagram of the experimental and numerical benchmark case.

Underwater slides are identified by translational failure, while underwater slumps are defined to undergo rotational failure (Schwab *et al.*, 1993).

3. Benchmark Validation

We present a benchmark case based on the sliding block experiments of previous researchers (Heinrich, 1992; Iwasaki, 1982; Watts, 1997; Wiegel, 1955). Figure 1 shows a straight incline with a planar beach inclined $\theta = 14^\circ$. The coordinate origin is at the undisturbed beach and the positive x-axis is oriented horizontally away from the shoreline. A semi-ellipse approximates the initial landslide geometry (Grilli and Watts, 1999; Watts and Borrero, this volume). The landslide specific density is $\gamma = 1.81$. The landslide length measured along the incline is $b = 1000$ m. The initial submergence at the middle of the landslide is $d = 261$ m while the maximum landslide thickness is $T = 52$ m. We performed this benchmark case experimentally, reduced in scale by a factor of 1000, and numerically with a boundary element model at the scale given here (Watts *et al.*, 2000; Grilli and Watts, 2001). We measured a slide initial acceleration of $a_o = 0.73$ m/s² with acceleration remaining more or less constant for the duration shown here. Figure 2 compares experimental and numerical results for landslide tsunami measurements at numerical wave gauges g_0 – g_3 (solid), as compared to scaled up laboratory measurements (dashed). Wave gauges are on the x-axis at $x = 1948$ m, $x = 2248$ m, $x = 2548$ m, $x = 2848$ m for g_0 , g_1 , g_2 , and g_3 , respectively. Experimental results represent the smoothed average of three replicates of identical experiments. Given the experimental errors involved, we consider our irrotational, inviscid numerical model of tsunami generation to be reasonably well validated.

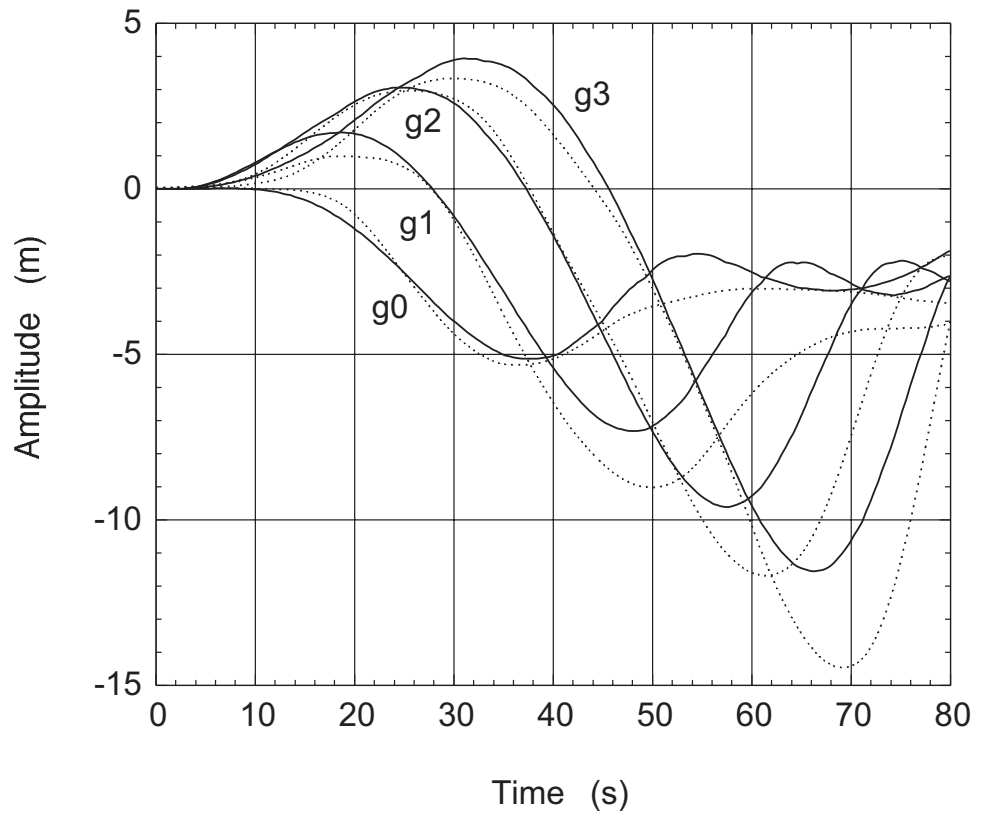


Figure 2: Experimental (dashed) and numerical (solid) results for the benchmark case.

4. Motion Versus Deformation

Tsunami generation in the shallow water wave limit occurs through vertical acceleration of some region of the ocean floor (Tuck and Hwang, 1972). Tsunami generation in an inviscid, irrotational numerical model occurs through gradients of the velocity potential at the free surface, which can arise from both horizontal and vertical landslide motions (Grilli and Watts, 1999). For such models, tsunamis can be generated by velocity in addition to acceleration, although acceleration is the only landslide motion experienced at early times. Watts and Borrero (this volume) describe two distinct center of mass motions: slides involving rectilinear failure of a thin layer of deformable silt or sand, and slumps involving deep failure of clay with residual shear strength restraining motion. Figure 3 compares tsunami generation by a landslide undergoing the center of mass motion of a slide with that of a slump at one numerical wave gauge above the landslide. With these distinct center of mass motions, we find that tsunami amplitudes and periods can differ by factors of 2–5 for identical landslide size, shape, and density. In both cases, the initial acceleration a_o is the most important measure of

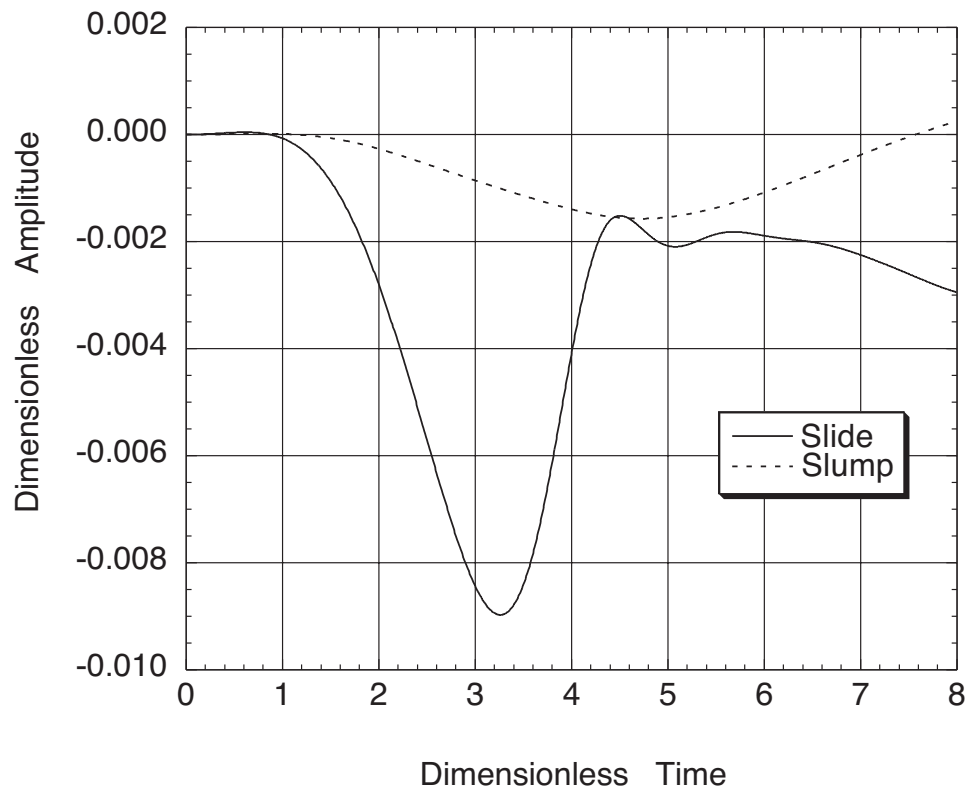


Figure 3: Comparison of underwater slide and slump generated tsunamis.

motion

$$a_o = \frac{s_o}{t_o^2} \quad (1)$$

where s_o is the characteristic distance of motion, and t_o is the characteristic time of motion (Watts, 1998, 2000). We ascribe the differences in tsunami features to the slide initial acceleration of $a_o = 0.60 \text{ m/s}^2$ when compared to the smaller slump initial acceleration of $a_o = 0.18 \text{ m/s}^2$ due to the restraining basal friction.

Watts (1997) found experimentally that the primary mode of landslide deformation is through extension parallel to the incline. Watts *et al.* (2000) found the same result for numerical simulations of deformable landslides performed with the model of Imamura and Imteaz (1995). For both experimental and numerical results, the rate of extension was constant (i.e., landslide length grew linearly in time) following an initial transient. The maximum landslide thickness T remained more or less constant over time. Therefore, self-similar landslide deformation can be described by a constant rate of extension Γ with dimension of inverse time. Watts *et al.* (2001) derive a maximum rate of landslide extension based on observations of actual

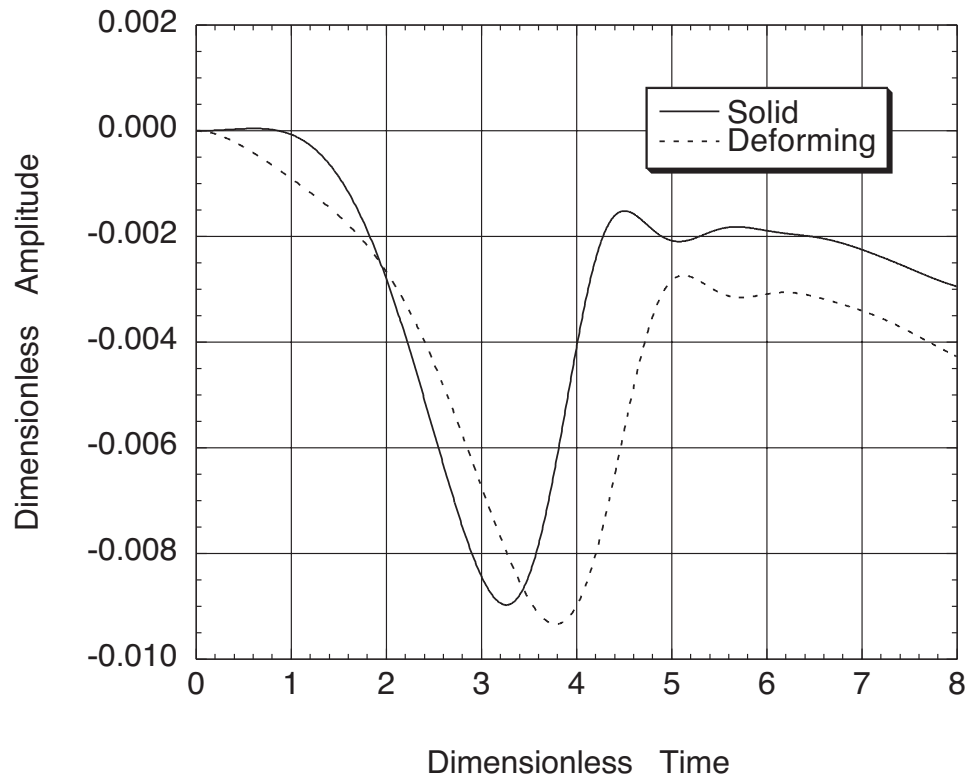


Figure 4: Comparison of solid and deforming underwater slide generated tsunamis.

landslide deposits

$$\Gamma_{\max} \approx \frac{\sqrt{\sin \theta}}{6} \sqrt{\frac{g}{b_o}} \quad (2)$$

where b_o is the initial landslide length and g is the acceleration due to gravity. Figure 4 demonstrates that the rate of deformation given by (2) changes the characteristic tsunami amplitude by less than 10% and has no significant effect on tsunami wavelength at one numerical wave gauge above the landslide. Wave generation at early times begins earlier and proceeds more slowly when deformation occurs, as seen on Fig. 4 and as noted by Watts *et al.* (2000). Center of mass motion appears to affect tsunami features more than landslide deformation (Watts *et al.*, 2001).

5. The 1998 Papua New Guinea Case Study

For the sake of brevity, we leave the known facts of the PNG event to be presented elsewhere (Watts *et al.*, this volume). Here, we develop and demonstrate a five-step tsunami simulation technique that reproduces almost all of the documented local tsunami features. A summary of the technique is presented in Synolakis *et al.* (2001), although we provide additional details and justification here.

5.1 Mass failure geology

We note that a push core taken by the Remotely Operated Vehicle (ROV) Dolphin 3K along the exposed failure plane revealed stiff biogenic mud (Tappin *et al.*, 2001). We also note our best estimate of the maximum thickness to length ratio $T/b = 15\%$ for the mass failure. These observations, in addition to bathymetric contours (Tappin *et al.*, 1999), indicate a typical cohesive slump that has traveled a small fraction of its length (Prior and Coleman, 1979; Schwab *et al.*, 1993; Turner and Schuster, 1996). The significant differences between cohesive slump motion and noncohesive slide motion account for the inability of earlier PNG landslide simulations to describe tsunami generation for this event (Tappin *et al.*, 1999, 2001).

5.2 Mass failure shape

We determined mass failure geometry from a combination of bathymetry data, sub-bottom profile records, and seismic reflection lines (Tappin *et al.*, 1999, 2001; Synolakis *et al.*, 2001). Both sub-bottom and seismic records revealed some motion along internal failure planes within the slump mass. However, the slump mass appears to have moved as one or at most two coherent units. We estimate a maximum thickness of $T = 600$ m, a width $w = 4$ km, and an initial length $b = 4.1$ km long (Tappin *et al.*, 2001; Synolakis *et al.*, 2001). Assuming parabolic profiles across both width and length, the slump involved a volume of about 4 km^3 of sediment. The largest known mass failures on earth are more than 1000 times more voluminous (Prior and Coleman, 1979; Edgers and Karlsrud, 1982; Turner and Schuster, 1996).

5.3 Mass failure motion

Since the slump center of mass motion is essentially decoupled from wave generation (Jiang and LeBlond, 1992; Watts, 2000), we solve equations of motion tailored to the local geology. We model the PNG slump as a rigid body rotating along a circular arc subject to external moments from added mass, buoyancy, gravity, and a constant residual shear stress (Batchelor, 1967; Bardet, 1997). We solve the linear differential equation for the angular displacement ϕ of a damped pendulum by invoking the small angle approximation

$$RV(\rho_b + C_m\rho_o)\frac{d^2\phi}{dt^2} \approx -(\rho_b - \rho_o)Vg\phi - wbS_u \quad (3)$$

where R is the radius of curvature, V is the slump volume, ρ_b is the bulk density, and ρ_o is the water density. The sediment residual shear strength S_u retards slump motion at all times (Bardet, 1997). We assume an added mass coefficient $C_m = 1$ (Batchelor, 1967; Watts, 2000). Multiplying the solution of (3) by the radius of curvature $R \approx 7$ km gives the slump center of mass position along the failure arc

$$s(t) = s_o \left[1 - \cos\left(\frac{t}{t_o}\right) \right] \quad (4)$$

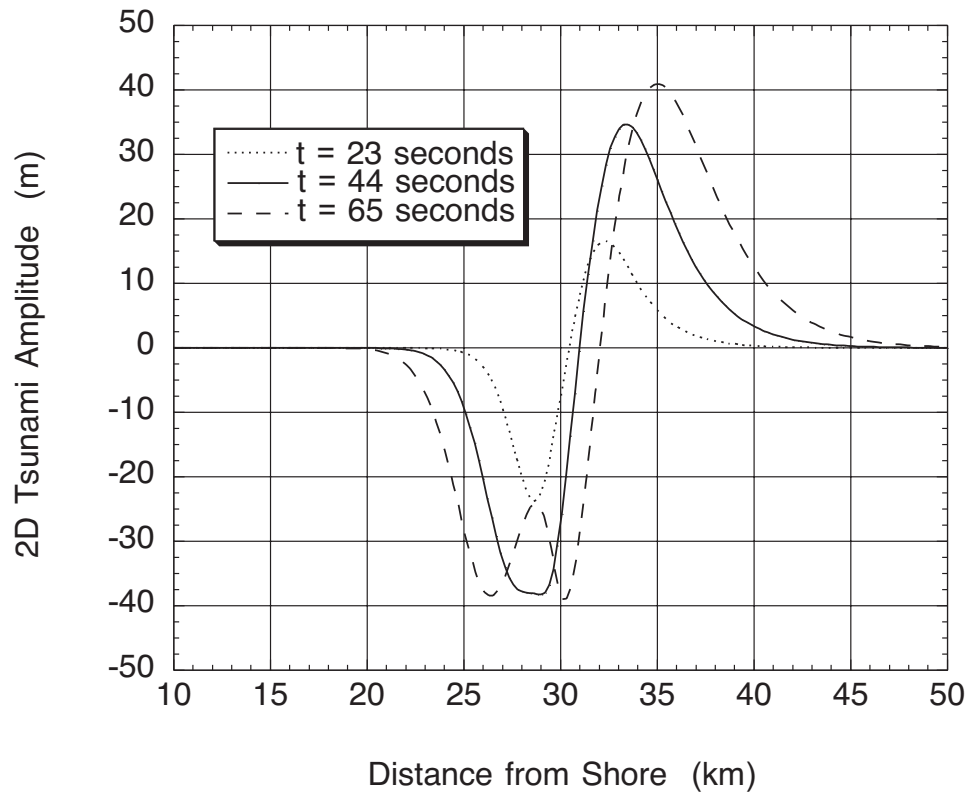


Figure 5: Profiles of the two-dimensional 1998 Papua New Guinea tsunami.

as a function of time subject to $s(0) = 0$ and $0 < t/t_o < \pi$. The characteristic distance and time of slump motion are found from (3) and (4) to be

$$s_o = \frac{R(\phi_f - \phi_i)}{2}, \quad t_o = \sqrt{\frac{R(\gamma + C_m)}{g(\gamma - 1)}} \quad (5)$$

which correspond to well known pendular motion. Based on the initial angle $\phi_i = -0.351$ and final angle $\phi_f = -0.065$ of the center of mass position expressed in radians as well as a slump specific density $\gamma = 2.14$, we calculate a characteristic distance of motion $s_o = 1$ km and a characteristic time of motion $t_o = 44$ s. These values correspond to an initial acceleration $a_o = s_o/t_o^2 \approx 0.51$ m/s² and maximum velocity $u_{\max} = s_o/t_o \approx 23$ m/s. These quantities differ by less than 3% with the exact solution of the nonlinear differential equation with fluid dynamic drag (Nayfeh and Mook, 1979).

5.4 Tsunami generation code

The strong horizontal component of slump acceleration suggests that a depth-averaged tsunami generation code may not be appropriate. A more rigorous evaluation of the long wave approximation is also possible. The initial slump depth of around $d \approx 1$ km yields a tsunami wavelength $\lambda = t_o\sqrt{gd} = 4.4$ km (Watts, 1998, 2000). The wavelength to depth ratio $\lambda/d \approx 4.4$ is about 5

times less than the criterion $\lambda/d > 20$ usually associated with shallow water waves. Therefore, we incorporate the center of mass motion into a complete fluid dynamic simulation of tsunami generation, employing the two-dimensional boundary element model of Grilli and Watts (1999) to solve irrotational and inviscid equations of fluid motion. This tsunami generation code is fully nonlinear and fully dispersive. The slump center of mass motion was prescribed by (4) and (5). Figure 5 reveals that tsunami amplitude consistently grew over a duration $t \approx t_o$ and ceased to grow significantly thereafter as waves propagated both towards shore and out to sea—the origin of this profile is at the shoreline as in Fig. 1. Watts (1998, 2000) has shown that t_o is both the duration of wave generation and the tsunami period. At the time $t = t_o$, we find a two-dimensional trough of -38.2 m and a peak of 34.7 m separated by a horizontal distance of almost exactly 4.4 km. We estimate the amplitude to depth ratio as $A/d \approx 0.035$ which provides an Ursell parameter $U = A\gamma^2/d^3 \approx 0.7$ indicative of both nonlinear and dispersive water waves. Our choice of tsunami generation code is justified.

The $w = 4$ km wide slump generated water waves in a depth $d \approx 1$ km, suggestive of essentially two-dimensional wave generation. We accounted for three-dimensional effects by assuming a parabolic transverse wave profile of width w in the absence of transverse wave propagation. During the time t_o of wave generation, the width of the wave will increase to approximately $(w + \lambda)$ and take on a form not dissimilar to

$$\frac{w}{w + \lambda} \operatorname{sech}^2 \left(\frac{3(y - y_o)}{w + \lambda} \right) \quad (6)$$

where y is measured perpendicular to the axis of slump failure. Conservation of mass dictates a reduction of $w/(w + \lambda) \approx 0.5$ in the overall tsunami amplitude due to transverse propagation (Watts *et al.*, 2001). The factor of three in the argument of (6) yields a relative wave amplitude of 1% at the transverse distance $y - y_o = w + \lambda$. We intend to reproduce these results using the three-dimensional model of Grilli and Watts (2001) in the near future.

5.5 Tsunami propagation code

We choose the accurate tsunami propagation code TUNAMI-N2 developed at Tohoku University to continue our case study (Imamura and Goto, 1988). We gridded the best available PNG bathymetry over a uniform spacing of 100 m. The tsunami generation behavior noted on Fig. 5 suggests that the time $t = t_o$ is an appropriate time to transfer results from the boundary element method code to the tsunami propagation code. We curve fit the shape in Fig. 5 with two Gaussians and modulated the two-dimensional shape with the functional form given in (6). We input the three-dimensional tsunami shape at $t = t_o$ as an initial condition for tsunami propagation

$$\eta(x, y) = \operatorname{sech}^2 \left(\frac{3(y - y_o)}{8.4} \right) \left(-35.71 \exp(-0.10128(x - 29.066 - x_o))^2 \right)$$

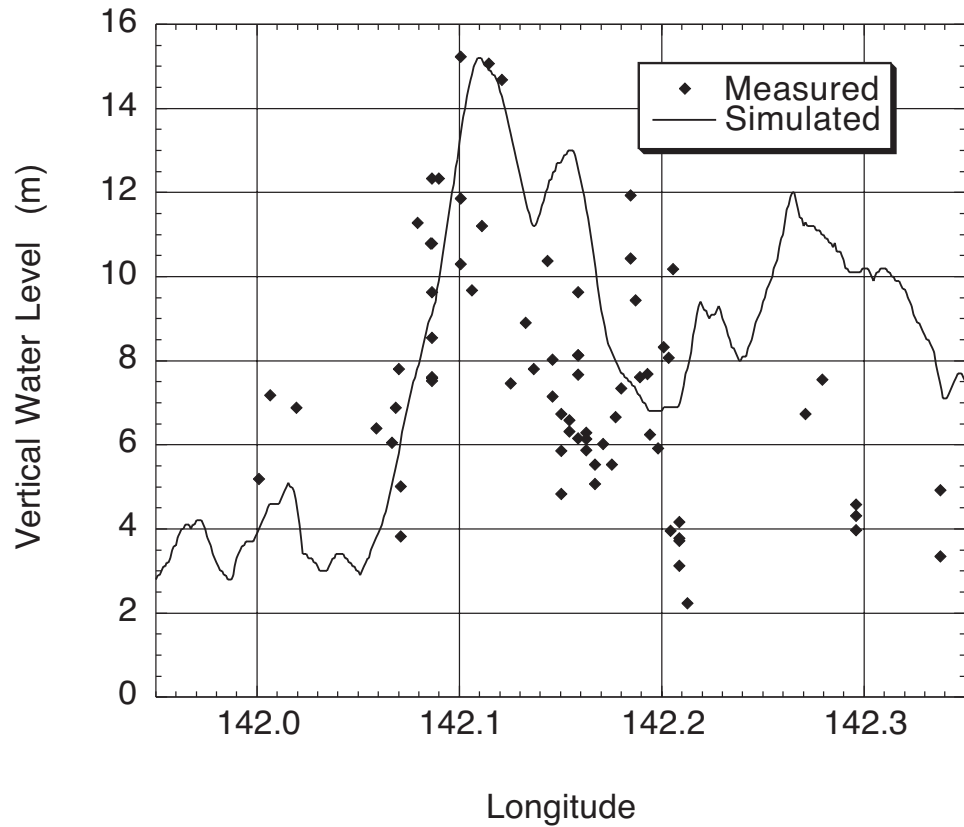


Figure 6: Comparison of measured and simulated water levels for the 1998 event.

$$+25.14 \exp(-0.051693(x - 31.709 - x_o)^2) \quad (7)$$

where x_o and y_o position the tsunami shape above the slump. For the function given in (7), the trough has an amplitude of -19.9 m while the peak has an amplitude of 16.4 m, where small errors in amplitude are introduced by the curve fit. We neglected water velocities when transferring the tsunami shape to the propagation code for two reasons. First of all, Watts (2000) demonstrated that landslide tsunamis partition most of their radiated energy into potential energy at times $t < t_o$. Second, the maximum water velocity is only 2% of wave celerity, or limited to 2 m/s, in the tsunami generation region. We estimate the ratio of kinetic to potential energy as being less than 1% for this tsunami.

Our maximum run-up results, based on the combined mass failure geology, geometry, and motion analyses linked with coupled generation and propagation codes, compare favorably with the field run-up measurements shown in Fig. 6. Agreement between simulated and measured longshore distribution of run-up is governed primarily by bathymetry and would improve with more accurate nearshore bathymetry. Landslide tsunami propagation is highly directional and resembles a rifle shot oriented along the axis of failure (Iwasaki, 1997; Tappin *et al.*, 2001). The waves that struck Sissano Lagoon

and Malol were part of the recoil from that rifle shot. Tsunami arrival times based on simulation results are 09:10 at Malol and 09:11 at Arop and Sissano. Eyewitness accounts from Malol describe tsunami arrival as soon as the approximately 45 s ground motion from the widely felt aftershocks at 09:09 ceased (Davies, 1998). The tsunami first attacked Malol, then Sissano soon afterwards, because of deep submarine canyons off of both villages. All simulations of tsunami generation within the source region predict first tsunami attack at Malol based on existing bathymetry. Tsunami arrival converged from both east and west on the sandy spit in front of Sissano Lagoon, also in agreement with eyewitness accounts and physical evidence (Davies, 1998; Kawata *et al.*, 1999).

6. Conclusions

We presented a landslide tsunami benchmark case and validated our boundary element method tsunami generation code with experimental results. We showed that tsunami generation by submarine mass failure requires foremost an accurate center of mass motion, whereas landslide deformation is a secondary consideration. The 1998 PNG event shows that submarine mass failures can generate large tsunamis that strike nearby coastlines shortly after a moderate earthquake. Our combined generation and propagation case study is part of a new and accurate technique to assess tsunami hazards from submarine mass failures. The technique couples tsunami generation and propagation codes. Future improvements of this technique will combine free surface elevation with depth averaged velocities. Another manner with which to couple generation and propagation codes is to pass information from one simulation to the other through time-dependent boundary conditions. Any coupling based on boundary conditions is necessarily more complicated because a wave leaving the generation region must be allowed to reenter the generation region at some later time. That wave, in turn, must be allowed to leave the generation region once again. Because of these additional propagation conditions, the tsunami generation code must have a quasi-transparent effect within the domain of the propagation code.

Acknowledgments. Most of this work was performed in close collaboration with Dave Tappin and Eli Silver. The authors are grateful for the financial support of Applied Fluids Engineering, Inc., and the Disaster Control Research Center at Tohoku University. PW is grateful for travel support from the NSF and FEMA through grants to the University of Southern California supervised by Prof. Synolakis. Gary McMurtry provided the sediment density off of PNG. Jose Borrero provided the PNG run-up measurements. Takeshi Matsumoto provided the Kairei PNG bathymetry while Philippe Heinrich provided the nearshore PNG bathymetry.

7. References

- Assier Rzadkiewicz, S., C. Mariotti, and P. Heinrich (1997): Numerical simulation of submarine landslides and their hydraulic effects. *J. Waterway Port Coast. Ocean Eng., ASCE*, 123(4), 149–157.

- Bardet, J.-P. (1997): *Experimental Soil Mechanics*. Prentice Hall, Upper Saddle River, NJ.
- Batchelor, G.K. (1967): *An Introduction to Fluid Dynamics*. Cambridge University Press, Cambridge, UK.
- Davies, H. (1998): *The Sissano Tsunami*. Published by the author, Port Moresby, PNG.
- Driscoll, N.W., J.K. Weissel, and J.A. Goff (2000): Potential for large-scale submarine slope failure and tsunami generation along the U.S. Mid-Atlantic Coast. *Geology*, in press.
- Edgers, L., and K. Karlsrud (1982): Soil flows generated by submarine slides: Case studies and consequences. *Nor. Geotech. Inst. Bull.*, 143, 1–11.
- Fine, I.V., A.B. Rabinovich, E.A. Kulikov, R.E. Thomson, and B.D. Bornhold (1998): Numerical modelling of landslide-generated tsunamis with application to the Skagway Harbor tsunami of November 3, 1994. *Proc. Tsunami Symp.*, Paris.
- Geist, E.L. (1998): Local tsunamis and earthquake source parameters. *Adv. Geophys.*, 39, 117–209.
- Goldfinger, C., L.D. Kulm, L.C. McNeill, and P. Watts (2000): Super-scale failure of the Southern Oregon Cascadia Margin. *Pure Appl. Geophys.*, 157, 1189–1226.
- Grilli, S.T., and P. Watts (1999): Modeling of waves generated by a moving submerged body: Applications to underwater landslides. *Eng. Anal. Boundary Elements*, 23(8), 645–656.
- Grilli, S.T., and P. Watts (2001): Modeling of tsunami generation by an underwater landslide in a 3D numerical wave tank. In press, *Proceedings of the 11th Offshore and Polar Engineering Conference*, Stavanger, Norway.
- Hammack, J.L. (1973): A note on tsunamis: Their generation and propagation in an ocean of uniform depth. *J. Fluid Mech.*, 60, 769–799.
- Hampton, M.A., H.J. Lee, and J. Locat (1996): Submarine landslides. *Rev. Geophys.*, 34(1), 33–59.
- Harbitz, C.B. (1992): Model simulations of tsunamis generated by the Storegga slides. *Mar. Geol.*, 105, 1–21.
- Heinrich, P. (1992): Nonlinear water waves generated by submarine and aerial landslides. *J. Waterway Port Coast. Ocean Eng., ASCE*, 118(3), 249–266.
- Imamura, F., and C. Goto (1988): Truncation error in numerical tsunami simulation by the finite difference method. *Coast. Eng. in Japan*, 31(2), 245–263.
- Imamura, F., and M.M.A. Imteaz (1995): Long waves in two-layers: Governing equations and numerical model. *Sci. Tsunami Hazards*, 13, 3–24.
- Imamura, F., and E.C. Gica (1996): Numerical model for tsunami generation due to subaqueous landslide along a coast. *Sci. Tsunami Hazards*, 14, 13–28.
- Iwasaki, S. (1982): Experimental study of a tsunami generated by a horizontal motion of a sloping bottom. *Bull. Earth. Res. Inst.*, 57, 239–262.
- Iwasaki, S. (1987): On the estimation of a tsunami generated by a submarine landslide. *Proc. Int. Tsunami Symp.*, Vancouver, B.C., 134–138.
- Iwasaki, S. (1997): The wave forms and directivity of a tsunami generated by an earthquake and a landslide. *Sci. Tsunami Hazards*, 15, 23–40.
- Jiang, L., and P.H. LeBlond (1992): The coupling of a submarine slide and the surface waves which it generates. *J. Geophys. Res.*, 97(C8), 12,731–12,744.
- Jiang, L., and P.H. LeBlond (1993): Numerical modeling of an underwater Bingham plastic mudslide and the waves which it generates. *J. Geophys. Res.*, 98(C6), 10,303–10,317.
- Jiang, L., and P.H. LeBlond (1994): Three-dimensional modeling of tsunami generation due to a submarine mudslide. *J. Phys. Oceanogr.*, 24, 559–573.
- Kawata, Y., and International Tsunami Survey Team members (1999): Tsunami in Papua New Guinea was intense as first thought. *Eos Trans. AGU*, 80(9), 101.

- Murty, T.S. (1979): Submarine slide-generated water waves in Kitimat inlet, British Columbia. *J. Geophys. Res.*, 84(C12), 7777–7779.
- Nayfeh, A.H., and D.T. Mook (1979): *Nonlinear Oscillations*. Wiley-Interscience, New York, NY.
- Plafker, G., R. Kachadoorian, E.B. Eckel, and L.R. Mayo (1969): The Alaska earthquake March 27, 1964: Various communities. U.S. Geol. Surv. Prof. Paper 542-G, U.S. Dept. of Interior, Washington, D.C.
- Prior, D.B., and J.M. Coleman (1979): Submarine landslides: Geometry and nomenclature. *Z. Geomorph. N. F.*, 23(4), 415–426.
- Schwab, W.C., H.J. Lee, and D.C. Twichell (1993): Submarine landslides: Selected studies in the U.S. exclusive economic zone. U.S. Geol. Surv. Bull. 2002, U.S. Dept. of Interior, Washington, D.C.
- Synolakis, C. E., J.-P. Bardet, J.C. Borrero, H. Davies, S.T. Grilli, E.A. Okal, E.A. Silver, S. Sweet, D.R. Tappin, and P. Watts (2001): Slump origin of the 1998 Papua New Guinea tsunami. *Proc. R. Soc. Lond.*, accepted.
- Tappin, D.R., T. Matsumoto, and shipboard scientists. (1999): Offshore surveys identify sediment slump as likely cause of devastating Papua New Guinea tsunami 1998. *Eos Trans. AGU*, accepted.
- Tappin, D.R., P. Watts, G.M. McMurtry, Y. Lafoy, and T. Matsumoto (2001): The Sissano, Papua New Guinea tsunami of July 1998—Offshore evidence on the source mechanism. *Mar. Geol.*, 175, 1–23.
- Tuck, E.O., and L.-S. Hwang (1972): Long wave generation on a sloping beach. *J. Fluid Mech.*, 51(3), 449–461.
- Turner, A.K., and R.L. Schuster (1996): *Landslides: Investigation and mitigation*. Special Report 247, Trans. Res. Board, National Academy Press, Washington, D.C.
- Verriere, M., and M. Lenoir (1992): Computation of waves generated by submarine landslides. *Int. J. Num. Methods Fluids*, 14, 403–421.
- Watts, P. (1997): Water waves generated by underwater landslides. Ph.D. thesis, California Institute of Technology, Pasadena, CA.
- Watts, P. (1998): Wavemaker curves for tsunamis generated by underwater landslides. *J. Waterway Port Coast. Ocean Eng.*, ASCE, 124(3), 127–137.
- Watts, P. (2000): Tsunami features of solid block underwater landslides. *J. Waterway Port Coast. Ocean Eng.*, ASCE, 126(3), 144–152.
- Watts, P., F. Imamura, and S.T. Grilli (2000): Comparing model simulations of three benchmark tsunami generation cases. *Sci. Tsunami Hazards*, 18(2), 107–124.
- Watts, P., S.T. Grilli, and C.E. Synolakis (2001): Tsunami generation by submarine mass failure. I: Wavemaker models. *J. Waterway Port Coast. Ocean Eng.*, ASCE, submitted.
- Wiegel, R.L. (1955): Laboratory studies of gravity waves generated by the movement of a submarine body. *Trans. AGU*, 36(5), 759–774.